

A NOVEL FLC AND MPC BASED HYBRID ENERGY STORAGE SYSTEM FED MICRO GRID

MANDALA NAGAJYOTHI¹, Smt. M. NAGA CHAITRA², Smt. P. SWATHI³

¹PG-Scholar, Department of EEE (Electrical Power Systems), JNTUA College of Engineering, Ananthapuramu., A.P., India.

²Assistant Professor (Adhoc), Department of EEE, JNTUA College of Engineering, Ananthapuramu., A.P., India.

³Assistant Professor (Adhoc), Department of EEE, JNTUA College of Engineering, Ananthapuramu., A.P., India.

Abstract: Microgrids are becoming very popular now-a-days throughout the world as they utilize renewable energy sources effectively. The intermittent nature of the main renewable energy sources has led to the proposal of several energy storage devices to increase the performance, stability, and reliability of microgrids.

Generally, the majority of researchers thought about using a PI controller for a PI's gain values can be difficult to modify, which increases inaccuracy and necessitates the addition of more passive components to account for frequency variations in the Hybrid Energy Storage System (HESS). In this work, we provide a Fuzzy Logic Control (FLC) and a Model Predictive Control (MPC) to govern three-level bidirectional DC/DC converters for grid connections to the Hybrid Energy Storage System of a DC microgrid (HESS). Examining the working modes of a three-level converter is the first step towards resolving its neutral point voltage imbalance. Battery and Ultra-Capacitor (UC) represented in a mathematical model is used to achieve this. Furthermore, the inner layer grid-connected converter control is proposed to be achieved using dynamic rolling optimization, while the outer layer steady state reference values are computed using the Model Predictive Control (MPC) technique. By using model predictive current control to align the current with the expected value, the inner layer eliminates system current ripple. The outer layer ensures voltage regulation and builds a current predictive model. A HESS's high- and low-frequency power distribution is realized via this cascaded architecture, which lacks filters and has two independent controllers. By considering the

imprecision and uncertainty of the input signal, FLCs can create control actions that are both resilient and adaptive. It can be difficult to use typical control procedures because of complex control systems or a lack of precise mathematical models. These systems usually make use of FLCs. Because FLCs may be quickly constructed using hardware or software, they are helpful for control applications in the real world. It makes it possible for two different various energy storage devices to allocate battery and UC power while controlling voltage independently. Finally, using Matlab/Simulink simulations, the efficacy of the HESS control approach is verified in a controller comparison and failure scenario

Keywords: Model Predictive Control (MPC), three-level DC/DC converter, hybrid energy storage system (HESS), and Fuzzy Logic Control (FLC)

I. INTRODUCTION

This research addresses DC distribution network dependability to investigate DC system development. The article first describes the important structures of the DC distribution Network. Next, the Markov model, k/n(G), and reliability evaluation model for power electronic equipment are developed. are applied to compute reliability characteristics of redundant components [1]. This investigation presented Adaptable DC power supply system may fix important issues with Shenzhen's urban power distribution networks, including Energy integrity management, grid-connected dispersed power production, DC load power supply. We

examined flexible DC power distribution technology's benefits [2].

BESS, or Battery Energy Storage System, is a workable remedy for renewable energy uncertainty as battery technology advances. BESS deterioration is a crucial element in BESS operations, often evaluated during planning. The Depth of Discharge (DoD) directly impacts BESS deterioration, which is intimately linked to the daily schedule [4]. This study initially examines Take into account variables like frequency, unit ramp, low frequency oscillation, and cascade failure to determine the role of energy storage in minimizing variance in renewable energy output. Furthermore examined are the grid-connected renewable energy fluctuation rate standard, mitigation topology, and kind of energy storage. The methods for allocation of hybrid energy storage and mitigation are then summarized and analyzed [5]. Ensuring power balance among RESs, load demand, and ESS requires the implementation of an effective control technique. When dispatching ESS power and decomposing system net power, a typical HESS control strategy employs the high-/low-pass filter approach. Super capacitors (SCs) and batteries are used as HESSs in our innovative integrated control method for photovoltaic-based dc grid systems [6]. The hybrid energy storage system makes use of super capacitors' benefits over batteries, including their longer cycling life, smaller capacity, and higher power density, to improve overall performance. Power electrical converters control energy storage systems so that charging and discharging are balanced. guaranteeing PV energy quality, enhancing functionality, prolonging lifespan, and bringing down PV power costs [7]. This paper presents the experimental inquiry, stability analysis, controller design, simulation research, and system operating concept. Bidirectional power flow integrating batteries and SC. When the SC system participates effectively in the suggested regulation mechanism, battery stress is reduced [8]. This research suggests a HESS for use in plug-in hybrid electric, hybrid, and electric cars that makes use of batteries and ultracapacitors. In the standard HESS

architecture, the ultracapacitor and the battery/dc link are interfaced via a bigger converter to fulfil real-time peak power demands. Nevertheless, in order to keep the ultracapacitor's voltage exceeds the voltage of battery under most city driving scenarios [9]. The suggested method makes use of virtual resistance for batteries and super capacitors as well as capacitance droop controllers, two complementary energy storage methods [10]. This work proposes model predictive control (MPC) for DC-DC converters that are bi-directional and operate at three levels. By creating a cost function, prediction model, and optimization process, DC voltage stability and midway voltage balance are optimized [11]. An experimentally confirmed predictive control system for a hybrid battery-ultracapacitor power source model is presented in this paper. First and foremost, the ultracapacitor current, voltage, battery current, and state of charge are all maintained within preset limits while using the suggested system [12]. By using this control method, the converter output generates a modulated waveform while maintaining the FCS-MPC properties. Simulate this approach and compare its results with the traditional FCS-MPC strategy to assess its feasibility [13].

Comparing this strategy to previous control systems, the research suggests the following advantages.

- 1) The suggested FLC and ANN control solution provides optimal power distribution between the UC and battery and faster DC-link voltage restoration when compared to traditional controllers.
- 2) Without filters, electricity is distributed at both high and low frequencies using this HESS management method. Overcharging or discharging of the battery is prevented by the slope limiter and outside voltage control.

II.HYBRID ENERGY STORAGE SYSTEM REPRESENTATION

A. HESS Topology

Figure 1 illustrates the HESS connected converter topology. The UC's three-level DC/DC converter, which is battery-powered, adjusts the bus voltage. The voltage applied to the bus side

input can be either the complete bus voltage (V_{dc}) or the halfway bus voltage ($V_{dc}/2$). Depending on the circumstances, supply voltage could be selected. By lowering switch voltage stress and inductor current ripples, this design lessens higher voltage DC bus power swings.

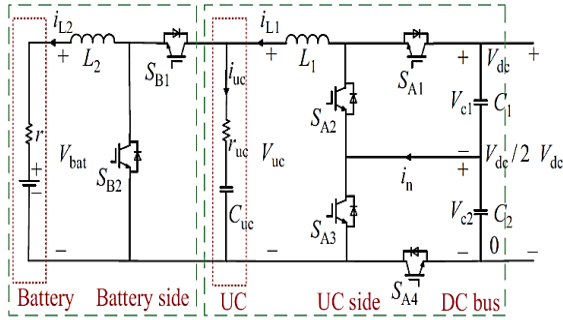


Figure 1: HESS Topology

The symbols V_{bat} and r represent the battery terminal voltage and internal resistance, respectively; the symbols UC voltage, resistance, and current, are V_{uc} , r_{uc} , and i_{uc} , respectively. i_{L1} and i_{L2} are the currents of inductor; C_{uc} is the UC capacitance; L_1 and L_2 control the battery and UC current; The DC bus voltage is V_{dc} ; switches S_{B1} , S_{B2} , and C_1 and C_2 are the same capacitors with voltages V_{c1} and V_{c2} , and S_{Ai} (i is 1 to 4) is the DC bus voltage.

B. Battery and UC represented in a Mathematical model

Battery types come with an integrated resistor in series with a constant voltage source. Voltage output:

$$V_{bat} = E - i_{bat}r \quad (1)$$

where i_{bat} is the current from battery and E is the consistent voltage source potential. UC may reduce microgrid power fluctuations because to its high power density [20]. It might lengthen the battery's life and lower its power burden [21]. An ideal series resistor and matching capacitor represent UC in DC microgrid systems. This basic model properly depicts UC

$$V_{uc} = V_c + i_{uc}r_{uc} \quad (2)$$

charging/discharging. Displaying UC's output voltage:

C. Neutral Point Voltage Balance Method

On the DC bus side, the voltage levels of the two capacitors, C_1 and C_2 , can actually differ significantly from one another. Neutral point current changes, also known as Neutral Point Voltage (NPV) variations, will cause an increase in the voltage stress on the capacitor and switch. Therefore, in order to preserve equilibrium, the distribution of on and off switches needs to be precise. V_{c1} as well as V_{c2} .

When $V_{dc}/2 < V_{uc} < V_{dc}$, capacitors C_1 and C_2 are linked to the system, and the whole DC bus voltage V_{dc} is the input voltage on the bus side, meaning that a neutral point current won't be produced in, S_{A2} and S_{A3} function in boost mode when $i_{L1} < 0$, and S_{A1} and S_{A4} operate in buck mode when $i_{L1} > 0$.

When $V_{uc} < V_{dc}/2$, only C_1 or C_2 is plugged in, creating a neutral point current within the system. Neutral Point Voltage (NPV) balancing mechanism must therefore be used in order to successfully balance V_{c1} and V_{c2} . Currently, $V_{dc}/2$ is the input voltage on the bus side. Capacitor charging and discharging state, as well as boost/buck mode operation of the system, are still unknown. by the value of i_{L1} . The values of V_{c1} and V_{c2} determine whether C_1 is connected to the system via S_{A1} and S_{A3} or C_2 is connected to the system via S_{A2} and S_{A4} .

III. MODEL PREDICTIVE CONTROL STRATEGY

The battery powers the UC, which in turn powers the DC bus. There are inner and outside voltage control layers in each part. The outside voltage control determines the expected inductor current required to maintain stable voltage. To accomplish the inner layer dynamic rolling optimization and the outer layer steady-state predictive value computation, the inner current control tracks the outer control's predictive value.

A. Strategy for Outer Voltage Control

Voltage control on the battery side A discrepancy between the rated reference voltage V_{ucref} and the

UC real voltage V_{uc} could have an immediate impact on the current i_{uc} . Following discharge and charging of the UC, the battery-side converter functions in boost mode otherwise, and in buck mode during the battery is charge and discharge. As per Kirchoff's current legislation (KCL), the converter's input current in Figure 2 is.

$$i_{in} = i_{L1} - i_{uc}$$

The reference current i_{L2ref} can be obtained in the following manner:

$$i_{L2ref} = i_{in} \times \frac{V_{uc}}{V_{bat}} \quad (3)$$

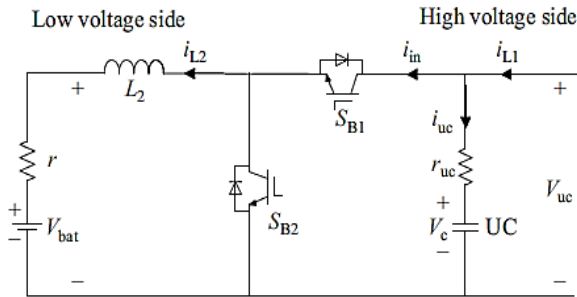


Figure 2: Battery Topology

Due to its huge capacitance, the UC voltage V_c fluctuates slightly under typical conditions. Accordingly:

$$i_{uc} = C_{uc} \frac{dV_c}{dt} \quad (4)$$

Later, the suggested approach limits UC current, and r_{uc} is extremely minimal. The comparable series resistor's voltage, r_{uc} , is limited to a tiny amount, therefore $V_c = V_{uc}$ is approximate. UC current:

$$i_{uc} = C_{uc} d \frac{V_{uc}}{dt} \quad (5)$$

According to (5), changing the UC voltage V_{uc} generates current i_{uc} . V_{uc} should be regulated around its rated value V_{ucref} , however it constantly deviates. Let the deviance change

linearly for a brief time. Only the UC current i_{uc} can modify V_{uc} . Since i_{uc} The reference prediction horizon N_{uc} cannot be made infinitely large. An integer coefficient that limits UC current. The sampling moment is k and the next instant is $k+1$. At $k+1$ moment, variables reflect predicted values. The sample frequency is $f_s = 1/T_s$, the sampling period from k instant to $k+1$. MPC controller calculation accuracy is positively associated with sampling frequency. High sampling frequencies make controller design more complicated. A reasonable value should be selected. According to [19], f_s is 20 kHz. The UC's rated voltage V_{ucref} may differ from the capacitor terminal voltage $V_{uc}(k)$ sampling value. The value must be reduced or increased to resemble V_{ucref} . $V_{uc}(k)$ will reach V_{ucref} in N_{uc} steps in Figure 3. Consider the ensuing moment $k+1$ to get equation:

$$\frac{V_{uc}(k) - V_{uc}(k+1)}{1} = \frac{V_{uc}(k) - V_{ucref}}{N_{uc}} \quad (6)$$

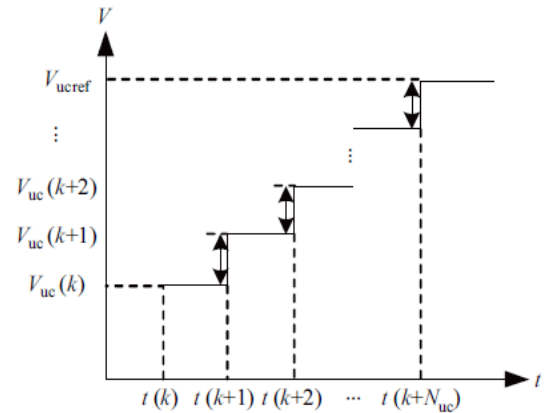


Figure 3: The reference prediction horizon N_{uc} design.

$$V_{uc}(k+1) = V_{uc}(k) + \frac{V_{ucref} - V_{uc}(k)}{N_{uc}} \quad (7)$$

$$\begin{aligned}
 i_{uc}(k+1) &= \frac{C_{uc}}{T_s}(V_{uc}(k+1) - V_{uc}(k)) \\
 &= \frac{C_{uc}(V_{ucref} - V_{uc}(k))}{N_{uc}T_s} \quad (8)
 \end{aligned}$$

UC predicted voltage at the following instant: The capacitor current i_{uc} ensures V_{uc} reaches V_{ucref} in N_{uc} steps. The present predictive value of UC is obtained by applying Euler's forward-difference law.

In accordance with (8), the following is represented as follows aiming for limiting the UC's current to less than 10 A due to its significant capacitance of the UC is around 29 F

$$i_{uc}(k+1) = \frac{C_{uc}(V_{ucref} - V_{uc}(k))}{N_{uc}T_s} < 10 \quad (9)$$

that is:

$$N_{uc} > \frac{C_{uc}(V_{ucref} - V_{uc}(k))}{10T_s} \quad (10)$$

Assuming that the UC's voltage is adequately controllable, suppose that the greatest difference between $V_{uc}(k)$ and V_{ucref} is 0.1 V. One can derive n_{uc} , which is around 5800. The current of reference i_{L2ref} as follows when expressing the inner current control:

$$\begin{aligned}
 i_{L2ref} = i_{L2}(k+1) &= i_{in}(k+1) \times \frac{V_{uc}(k)}{V_{bat}(k)} \\
 &= (i_{L1}(k) - i_{uc}(k+1)) \times \frac{V_{uc}(k)}{V_{bat}(k)} \quad (11)
 \end{aligned}$$

The sampling voltage and current determine the predictive current $i_{L2}(k+1)$. This current is the inner current control reference current i_{L2ref} . Model predictive current control (MPCC) calculates d_{bat} . The battery-side control govern is presented in Figure 4. The govern structure for the UC visualized in Figure 5. And Figure 6 depicts the MPCC control block schematic.

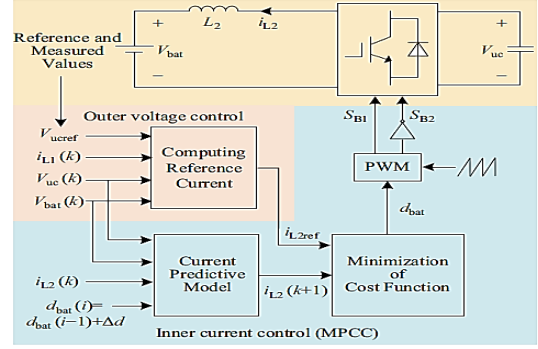


Figure 4: The battery control structure

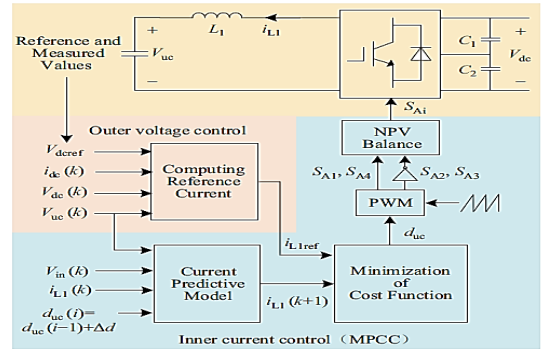


Figure 5: The UC control structure

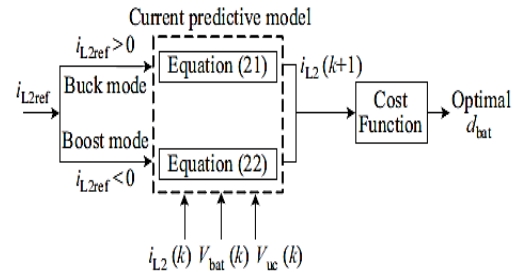


Figure 6: MPCC control block diagram for the battery

Fuzzy Logic Controller

FLC control systems reason about uncertain or inaccurate data using fuzzy logic. Expert systems like these can regulate industrial processes, consumer gadgets, and robots. Fuzzy arithmetic logic facilitates reasoning with imperfect or unclear data. LotfiZadeh invented it in the 1960s because many real-world issues contain imprecise and unpredictable information that classical logic cannot represent. Fuzzy logic uses fuzzy sets, which allow partial membership, or degrees of membership, instead of binary sets. FLCs are beneficial in systems with uncertain inputs and outputs that alter over time. FLCs can reason about input signal uncertainty and imprecision to develop resilient and adaptive control actions. Complex control systems or lack of exact mathematical models make standard control techniques challenging to execute. FLCs are typically utilized in these systems. FLCs are useful for real-world control applications because they may be built quickly utilising software or hardware. Automotive engineering, robotics, consumer electronics, medical equipment, traffic control, and financial modelling have used FLCs effectively.

Artificial Neural Network

An example of a control system that employs an artificial neural network (ANN) to manage a system or process is an ANN controller. With its networked artificial neurons that can adapt to changing circumstances, the ANN controller is a computational model created to mimic the functioning of the human brain.

Sensors measuring temperature, pressure, or speed, among other aspects of the system under control, provide input signals to the ANN controller. After processing these inputs, the ANN produces an output signal that is delivered to an actuator or other control device to modify the behavior of the system.

Robotics, self-driving cars, and health care and many more uses for ANN controller. They are especially helpful in scenarios when the system under control is intricate and challenging to model with conventional control methods.

ANN controllers' capacity to pick up new skills and adjust to shifting circumstances is one of their benefits. The ANN is fed input-output pairs during the training phase, and it modifies its weights and biases to reduce the error between the expected and actual outputs. The ANN can then be used to modify the behavior of the system in real-time by using this process to learn the best control policy for the system it is controlling.

IV.RESULTS AND DISCUSSION

The following five scenarios are simulated to confirm the efficacy of the FLC and ANN control methods: A) altering the step load; B) altering the control parameter; C) UC short-circuit fault; D) taking into account changes in photovoltaic power; E) comparing using the LPF method

A. Step Load Changes

The starting Considering the system's step load changes, the load is 1000 ohms and the DC loads 200 ohms and 100 ohms are connected to the bus in parallel at $t=0.2s$ and $t=0.4s$, respectively. The DC bus voltage and the UC voltage responses are watched for when using the FLC and ANN control methods.

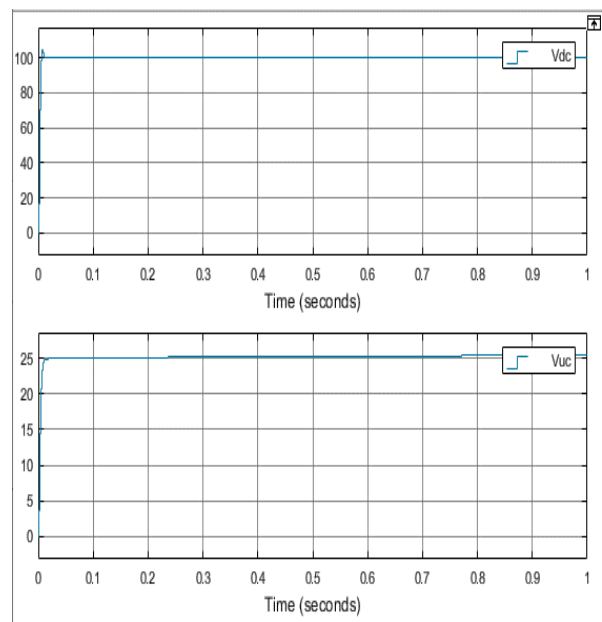


Figure 7: Bus Voltage and UC Voltage for FLC

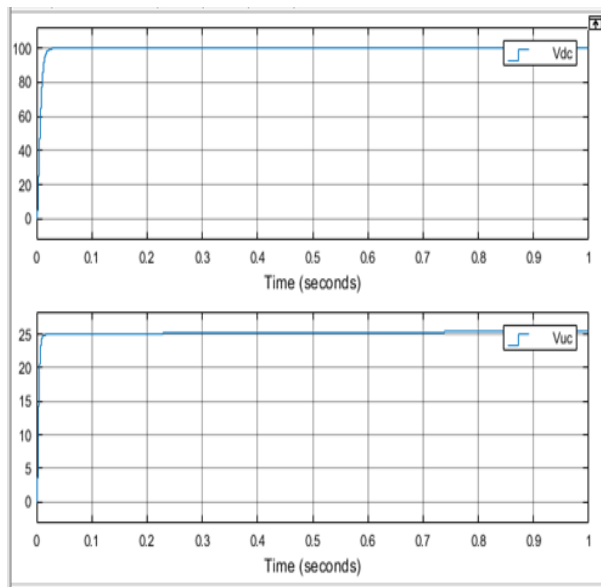


Figure 8: Bus Voltage and UC Voltage for ANN

It is evident that the system's dynamic performance under FLC & ANN controller is better compared to Conventional Controllers.

B. Changing Controller Parameter

The variations in load remain unchanged from those in A. Step load changes at causing the battery's power response at $t=0.4s$ is noted for FLC and ANN controllers

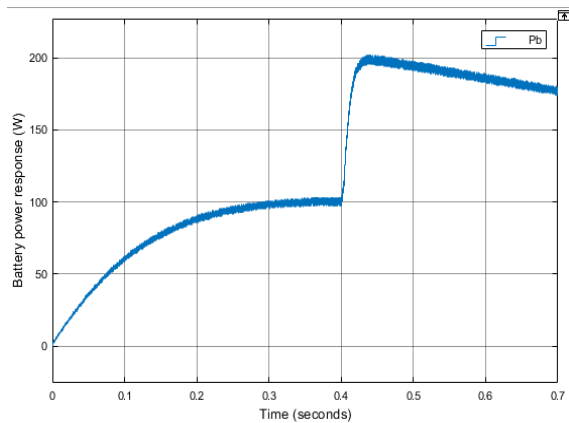


Figure 9: Power Response of Battery for FLC

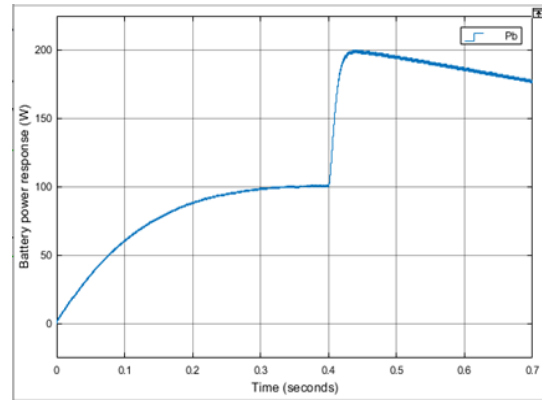


Figure 10: Power Response of Battery for ANN

C. UC Short-circuit Fault

In light of the UC's short-circuit defect in the HESS, the bus's reaction and the UC voltage under the FLC and ANN methods are noted. In typical operation, at $t=0.3s$, the UC has a short-circuit problem that is resolved in 0.05 seconds. Figures 11 and 12 show the voltage variations of the DC bus and the UC. The simulation findings, as seen in Figures 11(a) and 11(b), reveal that the UC short-circuit problem causes both the UC and bus voltages to drop sharply at $t=0.3s$. In 0.05 seconds, the mistake has been resolved. As the voltage of grid begins to increase once more, the UC's begins to recharge. As seen in Figures 12(a) and 12(b), the UC's huge capacity means that it takes a while to attain the first steady state. The findings demonstrate that the system under the control of the FLC and ANN controller may still be brought back to normal operation following the removal of the UC short-circuit problem.

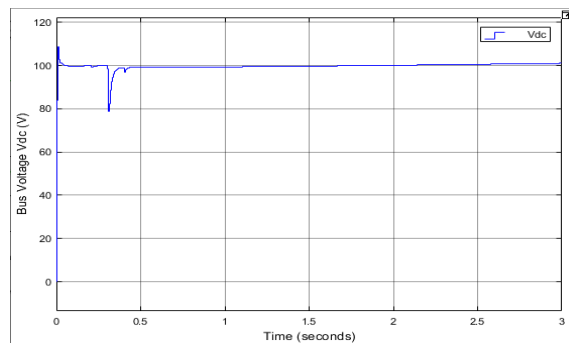


Figure 11(a): Bus Voltage when short circuit fault occurs in the UC for FLC

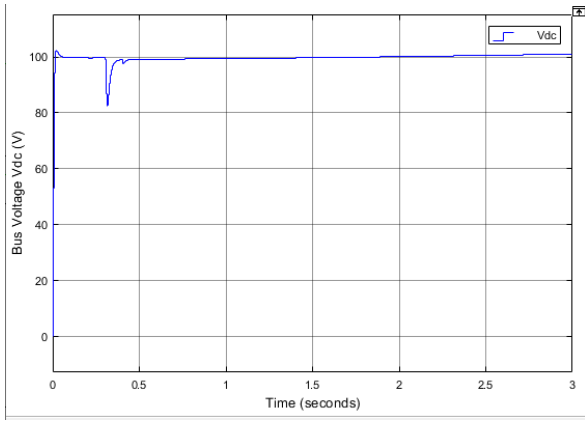


Figure 11(b): Bus Voltage when short circuit fault occurs in the UC for ANN

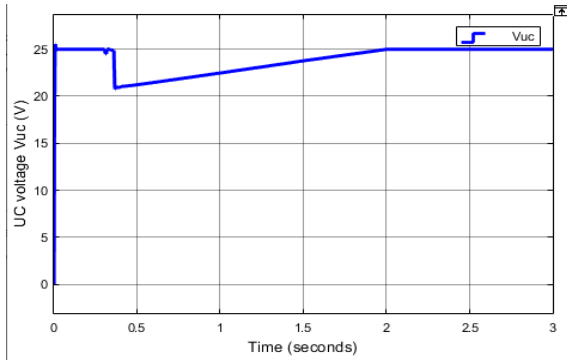


Figure 12(a): Voltage of the UC when short circuit fault occurs for FLC

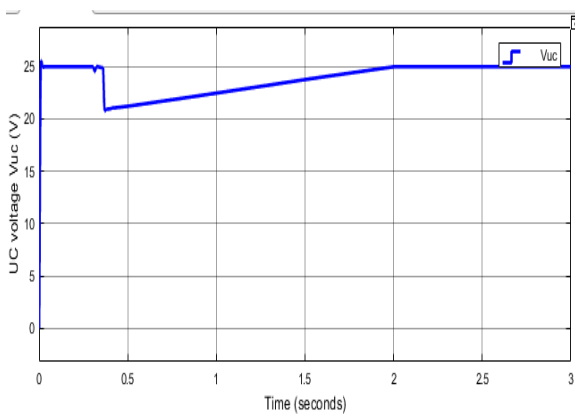


Figure 12(b): Voltage of the UC when short circuit fault occurs for ANN

D. Changes in Photovoltaic Power

First, 1000 is the load, followed by the application of 100 and 50 DC loads in tandem. During $t=0.5$ and 1 seconds, in that order. Additionally, at $t=0$, variable photovoltaic (PV) electricity is introduced. The Power generated by the PV module spans from 0 to 955 W at its maximum, as illustrated in Figure 13.

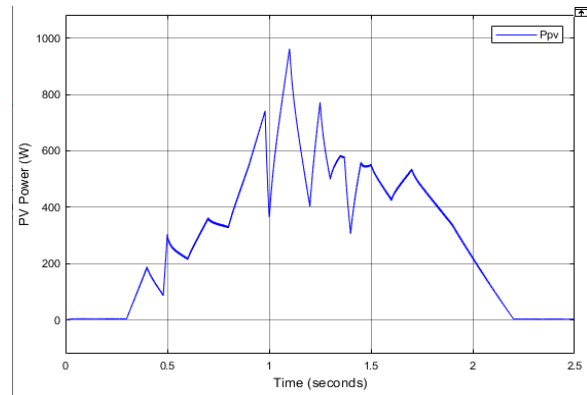


Figure 13: PV Module Power Output for FLC

Figure 13 and Figure 14 illustrates the effects of loads and variations in Photo Voltaic power on the UC and voltage of the DC bus and contrasts the ANN and FLC controllers.

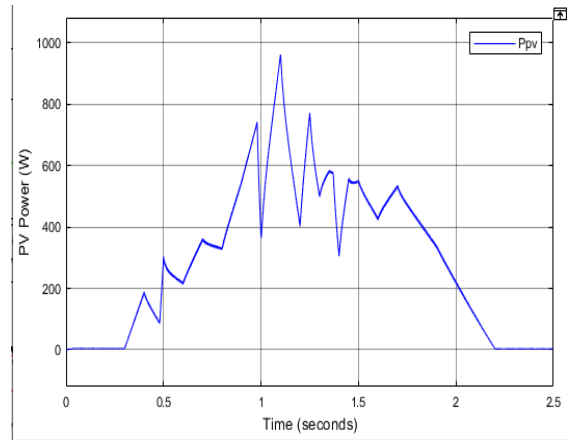


Figure 14: PV Module Power Output for ANN

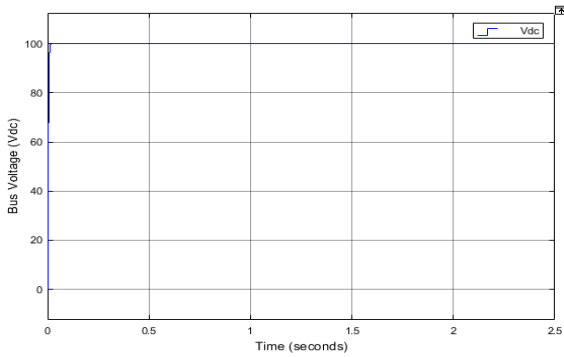


Figure 15(a): The bus voltage response for FLC

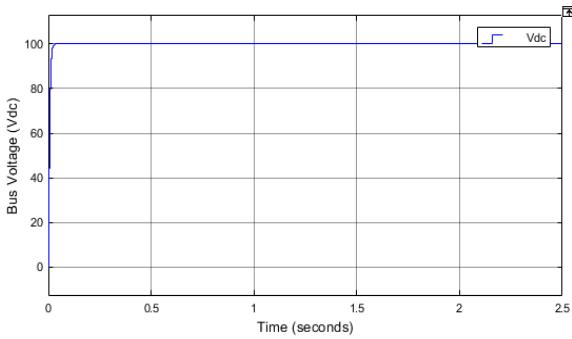


Figure 15(b): The bus voltage response for ANN

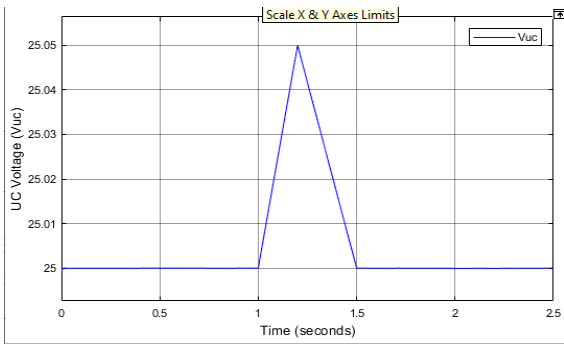


Figure 16(a): UC Voltage response for FLC

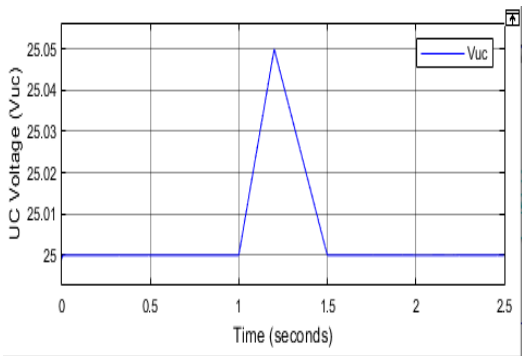


Figure 16(b): UC Voltage response for ANN

It can be seen that FLC and ANN controllers can guarantee the three-level converter's NPV balance in Figure 17(a) and Figure 17(b). When the reference current is closely followed by the actual current, there are little current ripples Figure 18(a) and Figure 18(b).

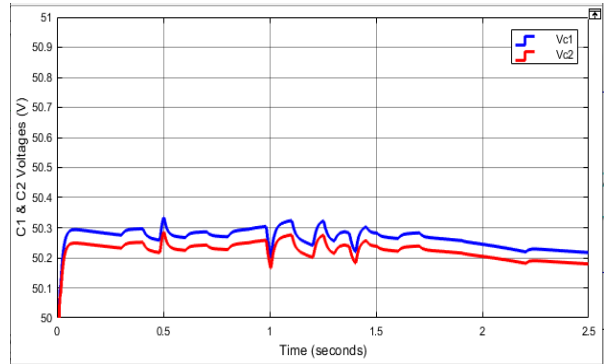


Figure 17(a): C1 and C2 Voltages for FLC

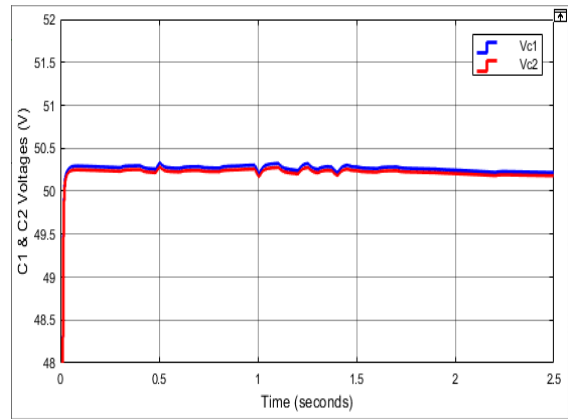


Figure 17(b): C1 and C2 Voltages for ANN

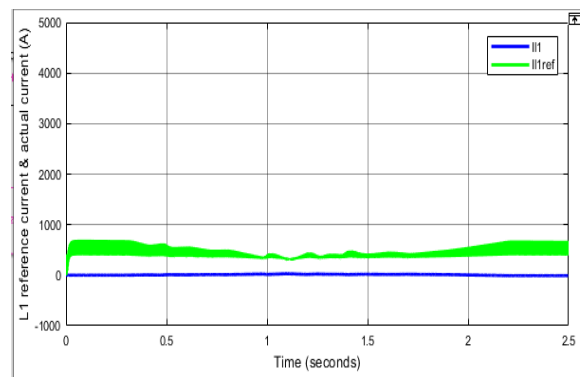


Figure 18(a): L1 reference current i_{L1ref} and actual current i_{L1} for FLC

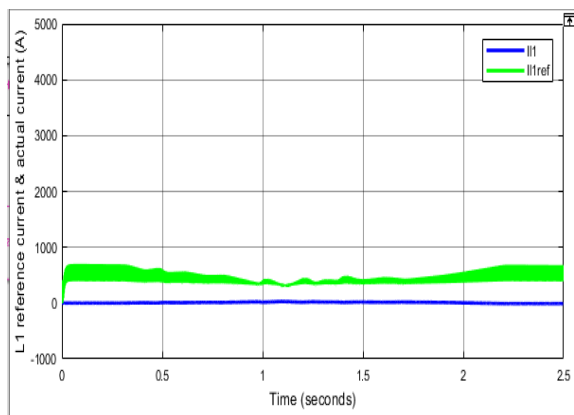


Figure 18(b): L1 reference current i_{L1ref} and actual current i_{L1} for ANN

E. Comparison using LPF Method

Replacing the current slope limiter with LPF can distribute high and low frequency power variations. Here, Figure 14 depicts a condensed block diagram. The recommended outer voltage control strategy is used to obtain i_{L1ref} , the total current reference for the complete HESS, which is divided for the battery and UC with LPF. The current demand's gradual variations (i_{L2ref}) is controlled by the system of batteries and the V_{uc} , V_{bat} . The compensating factor is applied following i_{L1ref} is transferred via LPF to acquire i_{L2ref} .

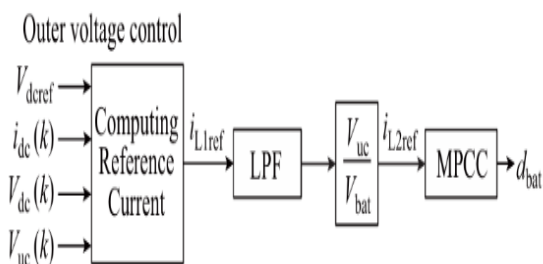


Figure 19: Block diagram with LPF

The power reactions of the energy storage units using these two methods are simulated under identical initial conditions for case A and D. The findings are illustrated in the Figure 20.

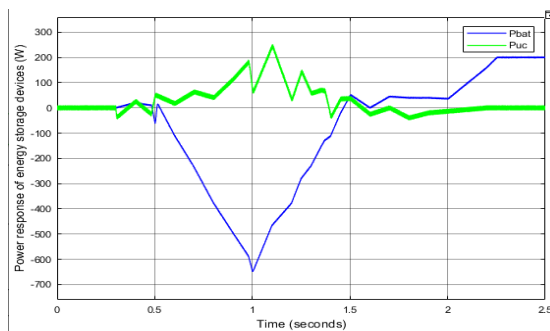


Figure 20(a): Photovoltaic Power Fluctuation with LPF

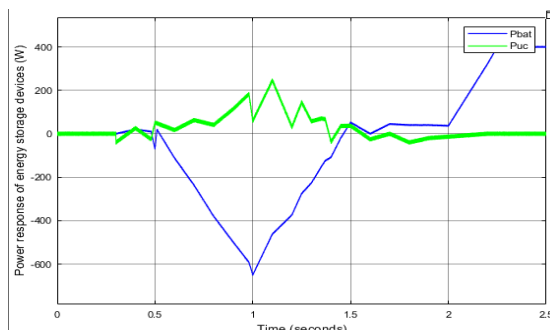


Figure 20(b): Photovoltaic Power Fluctuation for FLC(without LPF)

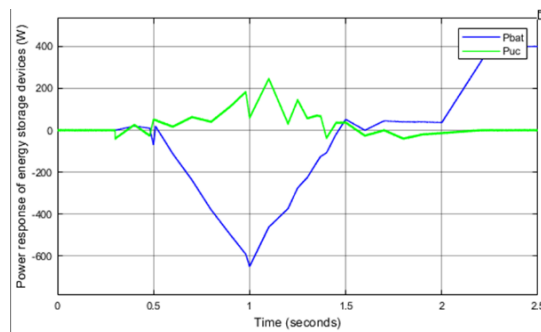


Figure 20(c): Photovoltaic Power Fluctuation for ANN(without LPF)

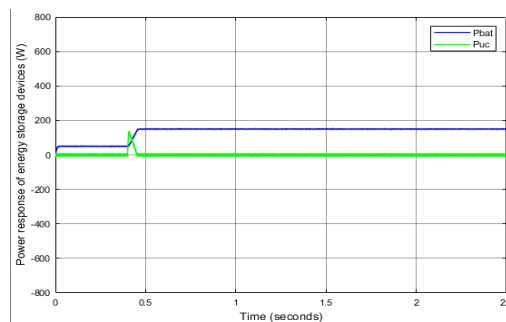


Figure 20(d): Step Load Change with LPF method

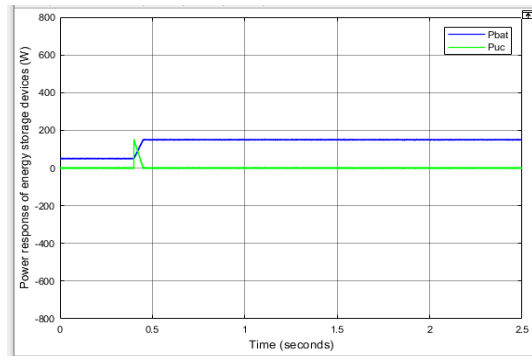


Figure 20(e): Step Load Change for FLC (Without LPF)

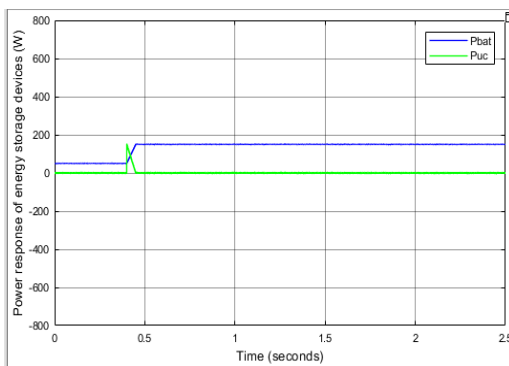


Figure 20(f): Step Load Change for ANN (Without LPF)

V. CONCLUSION

Based on theoretical research and simulation validation, this article discusses the efficacy of the suggested FLC and ANN approach and the benefits. Features a bidirectional DC/DC converter with three levels for use with UC and batteries. After a two-stage boosting construction, the battery can absorb changes in higher voltage levels while keeping the grid voltage constant. MPC system take more computational time and complexity of system is high, to overcome these drawbacks FLC and ANN controllers are used. The Intelligent controllers takes into account several state variables at each sample moment and eliminates the tiresome task of setting parameters, in comparison to conventional

controllers. This FLC and ANN approach enhances battery response and the hybrid energy storage system's dynamic performance features. Finally, the system can disperse power variations without the need for filters, and battery life is increased while the control structure is adjusted.

REFERENCES

1. Reliability evaluation of DC distribution power network, D. Liang, C. Y. Qin, S. Y. Wang, and H. M. Guo, Proceedings of 2018 China International Conference on Electricity Distribution, Tianjin, 2018, pp. 654–658.
2. The research status and future prospects of control and protection technologies for DC distribution networks are discussed in Z. Huang, J. Ma, J. Zeng, and others' work published in the Proceedings of the 2014 China International Conference on Electricity Distribution, Shenzhen, September 2014, pp. 1488–1493.
3. In the CSEE Journal of Power and Energy Systems, volume 3, issue 1, pages 101–113, March 2017, Joshi, K. A., and Pindoriya, N. M., "Case-specificity and its implications in distribution network analysis with increasing penetration of photovoltaic generation."
4. "Multiobjective chance-constrained optimal day-ahead scheduling considering BESS degradation," CSEE Journal of Power and Energy Systems, vol. 4, no. 3, pp. 316–325, Sep. 2018, Y. Xu, T. Y. Zhao, S. Q. Zhao, J. H. Zhang, and Y. Wang.
5. "Overview of energy storage in renewable energy power fluctuation mitigation," Y. Sun, Z. Zhao, M. Yang, D. Jia, W. Pei, and B. Xu, CSEE Journal of Power and Energy Systems, vol. 6, no. 1, pp. 160–173, Mar. 2020.
6. "Validation of faster joint control strategy for battery and supercapacitor-based energy storage system," IEEE Transactions on Industrial Electronics, vol. 65, no. 4, pp. 3286–3295, Apr. 2018, U. Manandhar, N. R. Tummuru, S. K. Kollimalla, A. Ukil, G. H. Beng, and K. Chaudhari.
7. In the Proceedings of the IEEE 8th International Power Electronics and Motion Control Conference, held in Hefei in 2016, pp.

- 2694–2698, H. J. Wang and J. C. Zhang conducted research on the charging/discharging control strategy of battery-super capacitor hybrid energy storage system in photovoltaic system.
8. Joint control of three-level DC-DC converter interfaced hybrid energy storage system in DC microgrids is described by U. Manandhar, B. F. Wang, X. N. Zhang, G. H. Beng, Y. T. Liu, and A. Ukil in *IEEE Transactions on Energy Conversion*, vol. 34, no. 4, pp. 2248–2257, Dec. 2019.
9. *IEEE Transactions on Power Electronics*, vol. 27, no. 1, pp. 122–132, Jan. 2012. J. Cao and A. Emadi, "A new battery/ultracapacitor hybrid energy storage system for electric, hybrid, and plug-in hybrid electric vehicles."
10. Q. W. Xu, X. L. Hu, P. Wang, J. F. Xiao, P. F. Tu, C. Y. Wen, and M. Y. Lee, "A decentralized dynamic power-sharing strategy for hybrid energy storage system in autonomous DC microgrid," *IEEE Transactions on Industrial Electronics*, vol. 64, no. 7, pp. 5930–5941, Jul. 2017.
11. Y. Mei, X. Q. Li, and Y. Y. Qi, "A model predictive control method for three-level bidirectional DC-DC converter in renewable generation system," in *Proceedings of the 2015 18th International Conference on Electrical Machines and Systems*, Pattaya, 2015, pp. 417–421.
12. B. Hredzak, V. G. Agelidis, and M. Jang, "A model predictive control system for a hybrid battery-ultracapacitor power source," *IEEE Transactions on Power Electronics*, vol. 29, no. 3, pp. 1469–1479, Mar. 2014.
13. M. Rivera, M. Perez, V. Yaramasu, B. Wu, L. Tarisciotti, P. Zanchetta, and P. Wheeler, "Modulated model predictive control (M2PC) with fixed switching frequency for an NPC converter," in *Proceedings of the 2015 IEEE 5th International Conference on Power Engineering, Energy and Electrical Drives*, Riga, 2015, pp. 623–628.
14. A. Dehghanzadeh, G. Farahani, H. Vahedi, and K. Al-Haddad, "Model predictive control design for DC-DC converters applied to a photovoltaic system," *International Journal of Electrical Power & Energy Systems*, vol. 103, pp. 537–544, Dec. 2018.
15. S. Wang, C. L. Xia, X. Gu, and W. Chen, "A novel FCS-model predictive control algorithm with duty cycle optimization for surface-mounted PMSM," in *Proceedings of the 7th IET International Conference on Power Electronics, Machines and Drives*, Manchester, 2014, pp. 1–6.
16. Y. H. Shan, J. F. Hu, K. W. Chan, Q. Fu, and J. M. Guerrero, "Model predictive control of bidirectional DC-DC converters and AC/DC interlinking converters—a new control method for PV-wind-battery microgrids," *IEEE Transactions on Sustainable Energy*, vol. 10, no. 4, pp. 1823–1833, Oct. 2019.
17. Y. H. Shan, J. F. Hu, Z. L. Li, and J. M. Guerrero, "A model predictive control for renewable energy-based AC microgrids without any PID regulators," *IEEE Transactions on Power Electronics*, vol. 33, no. 11, pp. 9122–9126, Nov. 2018.
18. Y. Mei, X. Q. Li, and Y. Y. Qi, "A model predictive control method for three-level bidirectional DC-DC converter in renewable generation system," *2015 18th International Conference on Electrical Machines and Systems (ICEMS)*, Pattaya, Oct. 2015, pp. 417–421.
19. X. N. Zhang, B. F. Wang, U. Manandhar, H. B. Gooi, and G. Foo, "A model predictive current-controlled bidirectional three-level DC/DC converter for hybrid energy storage system in DC microgrids," *IEEE Transactions on Power Electronics*, vol. 34, no. 5, pp. 4025–4030, May 2019.
20. A. Lahyani, P. Venet, A. Guermazi, and A. Troudi, "Battery/ supercapacitors combination in uninterruptible power supply (UPS)," *IEEE Transactions on Power Electronics*, vol. 28, no. 4, pp. 1509–1522, Apr. 2013.
21. W. Li and G. Jo'os, "A power electronic interface for a battery supercapacitor hybrid energy storage system for wind applications," in *Proceedings of 2008 IEEE Power Electronics Specialists Conference*, Rhodes, Jun. 2008, pp. 1762–1768.